

# Advanced hybrid plasmonic nano-emitters using smart photopolymer

DANDAN GE,<sup>1</sup>  ALI ISSA,<sup>1</sup>  SAFI JRADI,<sup>1,3</sup> CHRISTOPHE COUTEAU,<sup>1</sup>  SYLVIE MARGUET,<sup>2</sup>  AND  
RENAUD BACHELOT<sup>1,4</sup>

<sup>1</sup>Light, Nanomaterials, Nanotechnologies (L2n) Laboratory, CNRS EMR 7004, Université de Technologie de Troyes, 12 rue Marie Curie, 10004, Troyes Cedex, France

<sup>2</sup>Université Paris Saclay, CEA, CNRS, NIMBE, F-91191, Gif sur Yvette, France

<sup>3</sup>e-mail: safi.jradi@utt.fr

<sup>4</sup>e-mail: renaud.bachelot@utt.fr

Received 9 February 2022; accepted 3 May 2022; posted 4 May 2022 (Doc. ID 455712); published 10 June 2022

The integration of nano-emitters into plasmonic devices with spatial control and nanometer precision has become a great challenge. In this paper, we report on the use of a smart polymer to selectively immobilize nano-emitters on specific preselected sites of gold nanocubes (GNCs). The cunning use of the polymer is twofold. First, it records both the selected site and the future emitters–GNC distance through plasmon-assisted photopolymerization. Second, because the polymer is chemically functionalized, it makes it possible to attach the nano-emitters right at the preselected polymerized sites, which subsequently recognize the nano-emitters to be attached. Since the resulting active medium is a spatial memory of specific plasmonic modes, it is anisotropic, making the hybrid nanosources sensitive to light polarization. The ability to adjust their statistical average lifetime by controlling the thickness of the nanopolymer is demonstrated on two kinds of nano-emitters coupled to GNCs: doped polystyrene nanospheres and semiconductor colloidal quantum dots. © 2022 Chinese Laser Press

<https://doi.org/10.1364/PRJ.455712>

## 1. INTRODUCTION

Organic and inorganic nano-emitters are used for many topical applications ranging from nano-optics and nano-photonics to biomedicine and cell biology [1–3]. When weakly or strongly coupled to metal nanoparticles, their key properties can be controlled: lifetime [4,5], quantum yield [6], fluorescence directivity [7], emission intensity [8], and spectral properties [9]. The integration of these hybrid nano-emitters as optical nanosources into photonic nanodevices is of interest for research and technological innovation due to their miniaturization and multi-applications.

However, the integration of the emitters near metallic nanostructures with spatial control and nanometer precision in the three space dimensions remains a challenge. In the simplest way, the emitters are dispersed randomly on the plasmonic structures, without any position control [10,11]. By adding a spacer layer, the separation distance between the emitters and metallic structures can be controlled along one direction [12–14]. To achieve 3D spatial control of emitters relative to metallic nanostructures, a method based on trapping emitters in an isotropic silica shell covering the entire metallic nanoparticles has been reported [15,16]. Scanning-based methods have been reported to study in a controlled way the coupling between emitters and metallic nanostructures [17,18]. The

DNA origami-assisted method, as a powerful approach, has been used to build special plasmonic nanoantennas and link together plasmonic nanostructures and nano-emitters [19–22]. For the structures that present a gap, including dimers and particle-film structures, DNA origami has proven to be able to place emitters, even a single one, within the gap [23–27]. In other words, DNA is generally used to both bridge particles together and attach nano-emitters. In the case of single metal nanoparticles, the whole surface of particles is functionalized. With this approach, it is thus difficult to control the anisotropy of the emitters' distribution around single plasmonic nanostructures. With the use of a DNA clamp, gold nanoparticles have been placed at three special positions around a single nanorod, but the DNA clamp and special capture strands on the clamp limit the shapes and size of the host nanostructures and it is hard to change the capture positions for a defined clamp [28]. In addition, DNA-based hybrid nanosystems are pretty fragile in the sense that, for the survival of DNA origami, one must be in a salty liquid environment, which limits the types of available metallic nanoparticles and requires complicated steps. This environmental requirement limits the use of this approach for direct integration into nanophotonic circuits. Although site-selective coating based on anisotropic chemical growth on metal nanostructures has been reported [29–32], there are still challenges in achieving anisotropic distribution of the emitters

themselves near metal nanoparticles. As a matter of fact, it is still a challenge to control the anisotropic spatial distribution of emitters in the vicinity of single metal nanostructures in the three space dimensions.

Near-field plasmonic photopolymerization has proven to be an effective technique to trap light-emitting quantum dots (QDs) and molecules inside polymer volumes that are integrated at electromagnetic hot spots [33,34]. The anisotropic distribution of emitters can be controlled by choosing the plasmonic mode used for nanophotopolymerization. However, since the emitters are initially randomly distributed inside the photopolymerizable formulation, the spatial distribution of the emitters is still not precise enough. For example, the distance between the nano-emitters and the metal nanoparticle in the structures of Ref. [33] is not controlled. In addition, because the emitter is pre-dispersed within the formulation, it is difficult to consider the influence of the curing laser on the emitter during the photopolymerization process, such as the two-photon absorption by the emitters, and the possible light force that may squeeze the emitters outward.

In this paper, we report on the use of a smart nano-polymer that allows us to address these issues. The smart nature of the polymer is twofold. First, it is a photopolymer that reticulates at the plasmonic hot spot of the metal nanoparticle, allowing one to keep the memory of the selected electromagnetic sites. This memory is spatially anisotropic and also decides the distance between the plasmonic nanostructure and the future nano-emitter to be attached. Second, it is chemically pre-functionalized to electrostatically recognize the nano-emitter that can get selectively attached to the pre-designed sites.

Our approach is actually based on the association of three controlled elements: plasmonic nanostructures, smart photopolymer, and nano-emitters.

## 2. EXPERIMENTAL SECTION

### A. Plasmonic Nanostructures

The plasmonic nanocavities used are 125 nm gold nanocubes (GNC) which are shown in Fig. 1(a) and are made by chemical synthesis using the method already described in detail in Ref. [35]. These cubes, deposited on a glass substrate coated with indium tin oxide (ITO), present a dipolar plasmon resonance at 670 nm in air, as shown by the blue curve in Fig. 1(b), and are suitable for resonant near-field two-photon polymerization [33].

### B. Smart Photopolymer

The photopolymer has been designed for plasmon-induced two-photon nanoscale polymerization [33,34], but has been modified: it is also a functionalized polymer that grabs the emitters to its surface by electrostatic interaction. In that way, we can control both the number of emitters attached to the polymer surface and the average emitter-metal surface distance by adjusting the thickness of the polymer on the plasmonic structure. The photosensitive formulation consists of 4.99 mmol of pentaerythritol triacrylate (PETA) monomer functionalized by 2.51 mmol of methyldiethanol amine (MDEA). 0.039 mmol of 2-isopropylthioxanthone (ITX) was added to absorb light and cause the interaction with MDEA to initiate the two-photon polymerization reaction and 1.13 mmol of mono-methyl ether of hydroquinone (MEHQ) inhibitor was added

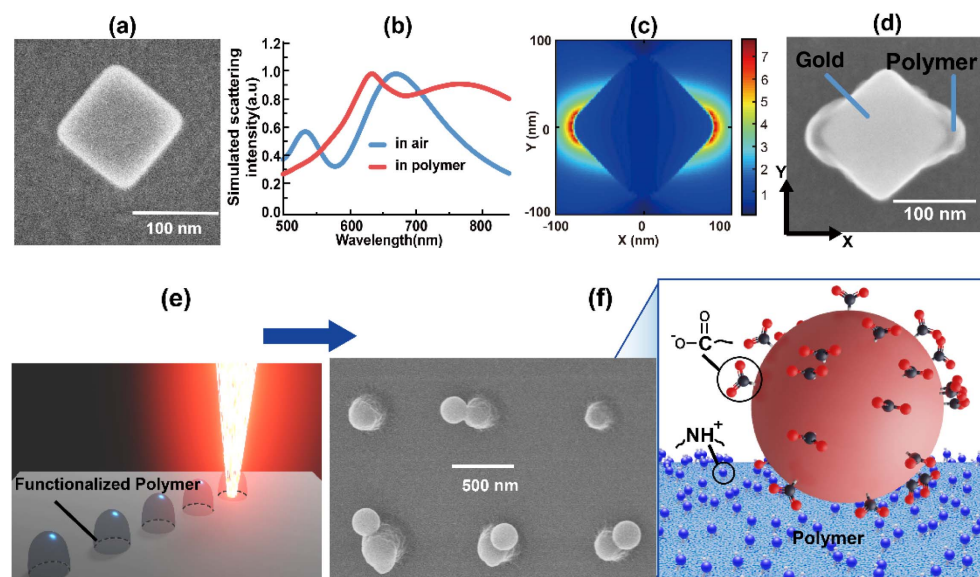


**Fig. 1.** GNC, nanoscale photopolymerization, and surface functionalization. (a) SEM image of a representative single GNC. (b) Calculated scattering spectrum of a single GNC of 125 nm, in air or photopolymer medium (refractive index = 1.48), on ITO-coated glass substrate (40 nm thickness of ITO layer with refractive index of 2). (c) FDTD map (at the middle sectional plane of the cube,  $\lambda = 780$  nm) of the field modulus in the vicinity of the GNC illuminated with an X-polarized plane wave. (d) SEM image of the hybrid nanostructure resulting from two-photon polymerization (TPP) triggered by the field shown in (c). (e) Illustration of the photopolymerization of mixture of PETA monomer functionalized by amine. (f) Left: SEM image of polymerized dots whose surface contains amine group. After immersion in a solution of negatively charged functionalized fluorescent doped polystyrene spheres (200 nm diameter), the fluorescent spheres attached on four of the six polymer dots by electrostatic interaction. Right: schematic representation of the electrostatic interaction.  $\text{NH}^+$  represents the positively charged protonated amine group.

to control the spatial confinement of the polymerization process. After photo reticulation and development, the polymer surface presents a high density of amino groups,  $10^8$  molecules per  $\mu\text{m}^2$  determined by the orange 2 test.

More information about the smart photopolymer can be found in Ref. [36]. The obtained polymer nanotemplates are intended to be immersed in acidic medium solution of negatively charged nano-emitters, resulting in the specific attachment of these nano-emitters on the polymer surface. In other words, during immersion, the negatively charged nano-emitters selectively assemble, by electrostatic interaction, on the positively charged functionalized polymer surface due to the presence of protonated amine groups [Fig. 1(f)].

### C. Nano-Emitters

The first considered nano-emitters are fluorescent polystyrene spheres (FPSs, Thermo Fisher Scientific) doped with light-emitting molecules. They are similar to those introduced in Fig. 1 but they are significantly smaller. Their average size is 45 nm. Their absorption spectrum presents a peak at 580 nm and the emission peak is at 620 nm (see Appendix B). Such FPSs were used by de Torres *et al.* to demonstrate plasmon-mediated fluorescence energy transfer on silver nanowires [37]. The authors deposited the FPSs by spin-coating and their spatial distribution was not controlled. The carboxylate-modified FPSs (Model F8793, FluoSpheres) used in this paper, are negatively charged and thus able to get selectively positioned to the functionalized polymer surface by electrostatic force.

Based on the three elements described above, advanced hybrid plasmonic nano-emitters can be made.

### D. Protocol to Fabricate Hybrid Plasmonic Nano-Emitters

The protocol for fabricating a hybrid plasmonic nano-emitter consists of two main steps, as shown in Appendix A (Fig. 6).

Step 1 consists of the fabrication of the functionalized nanopolymer on the GNC surface by plasmon-triggered polymerization at 780 nm [33,34,38]. This wavelength efficiently excites the GNC plasmon when it is later surrounded by the liquid photopolymer, as shown by the red curve in Fig. 1(b), and is efficiently absorbed by the ITX that is used as a two-photon absorber [39]. The photopolymerization occurs specifically at the electromagnetic hot spots, when the near-field intensity exceeds a certain intensity threshold [40,41]. During this step, the selected nanoscale sites are thus recorded by the polymer. After exposure, the deposited polymer volume is revealed through separately rinsing with acetone and isopropanol for 10 min. Figure 1(d) illustrates a typical hybrid nanocube, revealed after rinsing, that results from nanopolymerization triggered by the plasmonic dipolar eigenmode excited with an *X* polarization parallel to the diagonal of the cube, as shown in Fig. 1(c). The process relies on the control of the incident intensity relative to the threshold dose (Dth) of two-photon polymerization. To get the result shown in Fig. 1(d), the incident laser dose was 40% of the threshold dose so that no polymerization occurs, except in the near field of the GNC, as illustrated in Fig. 1(c), where the local dose gets higher than Dth through plasmon enhancement.

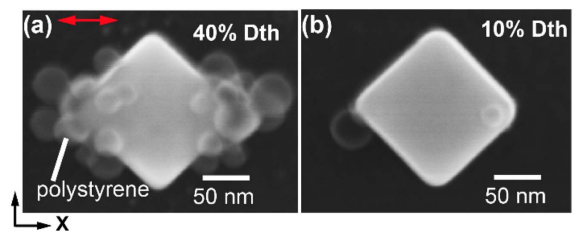


**Fig. 2.** SEM images of the hybrid FPSs attached nanostructures fabricated using energy dose of (a) 40% and (b) 10% of threshold during Step 1. The red arrow in (a) indicates the polarization direction of the excitation laser used for polymerization during Step 1.

The experimental configuration used for this step is shown in Appendix A, Fig. 7.

Step 2. After Step 1, the sample is immersed into the FPS solution for 40 min. The FPSs were stabilized by carboxylic acid and have negative charges on their surface. During immersion, and due to the presence of amine groups on the polymer (positive charges), FPSs get attracted by the polymer, leading to the selective attachment of FPSs on its surface by electrostatic interaction. During this step, the prerecorded smart polymer gets revealed by selectively attaching nano-emitters.

### E. Selective Attachment of Fluorescent Spheres at the Nanocube Corners

By adjusting the dose used in Step 1, we were able to control the nanopolymer's thickness and thus the average distance between the GNC surface and the nano-emitters to be attached. At the same time, the increased thickness of polymer leads to an increased number of grafted emitters. Figure 2 illustrates this point: two different volumes of the polymer lead to a large change in the number of attached FPSs. The effect of the dose on the volume of the polymer is clearly shown in Appendix C, Figs. 9 and 10. The selective immobilization of FPSs at the two corners of GNC is here successfully demonstrated. The excitation laser used for two-photon polymerization was *X*-polarized, resulting in two lobes of smart polymer that took the shape of the local plasmonic field, shown in Figs. 1(c) and 1(d). In Figs. 2(a) and 2(b), two identical GNCs have been polymerized with two incident doses at 780 nm: 40% and 10% of Dth, respectively (Step 1). Step 2 results in a hybrid FPS/GNC with a number of FPSs at each cube corner, which is strongly dependent on the dose initially used for Step 1: from a tenth of FPSs [Fig. 2(a)] to a few FPSs [Fig. 2(b)]. More examples can be found in Appendix C, Fig. 9. Appendix H deals with the control of the number of emitters that can attach to the polymer lobes. This number depends on the concentration of emitters in the solution, the size of the emitter, the size of the integrated polymer area, and the immersion time. In particular, Figs. 2, 9, and 16 illustrate the importance of the latter two.

## 3. RESULTS AND DISCUSSION

### A. Photoluminescence Properties of the Resulting Hybrid Nano-Emitters

Under 532 nm excitation, the fluorescent signal was collected through a 650/150 nm bandpass filter (FF01-650/150-25, Semrock). The fluorescence spectrum from the hybrid

FPS–GNC nano-emitter is shown in Fig. 3(a). In Fig. 3(b), the time trace of fluorescence intensity obtained during 50 s shows no blinking and a pretty good stability of the fluorescence intensity. This is due to the large number of dyes inside each FPS giving out an ensemble signal and the protective environment inside the polystyrene bead isolating the system from the unstable effects from the external environment.

These hybrid nanostructures have an anisotropic nanoscale spatial distribution of FPSs that contributes to the polarization sensitivity of their fluorescence intensity. This feature is illustrated in Fig. 3(d). The 532 nm excitation light was linearly polarized with a polarization angle shown in Fig. 3(c). The considered single hybrid nano-emitter has been fabricated during Step 1 using 40% of Dth. In Fig. 3(d), the fluorescence intensity decreases when the polarization angle of the excitation laser varies from 0° to 90° and increases when the polarization changes from 90° to 180°. The fluorescence intensity finally goes back to the same intensity level as the intensity of 0°. The switch from a high emission signal to a weak emission signal is realized by rotating the polarization direction, and a signal contrast  $\delta$  of about 0.5 is obtained. In Fig. 3(b), the cosine-like function, reminding us of the Malus law, is not due to the polarization sensitivity of the GNC. Rather, it is due to anisotropic spatial distribution of the active medium permitted by the smart polymer. More data on the polarization sensitivity can be found in Appendix D (Fig. 11).

**B. Control of the Average Gap between GNC and Nano-Emitters and Resulting Purcell Factor**

The spatial elongation of the nanopolymer during Step 1 can be controlled by incident energy doses [31,32]. Energy doses ranging from 5% to 70% of Dth were used to fabricate hybrid FPS-attached hybrid plasmonic nanostructures (Step 1).

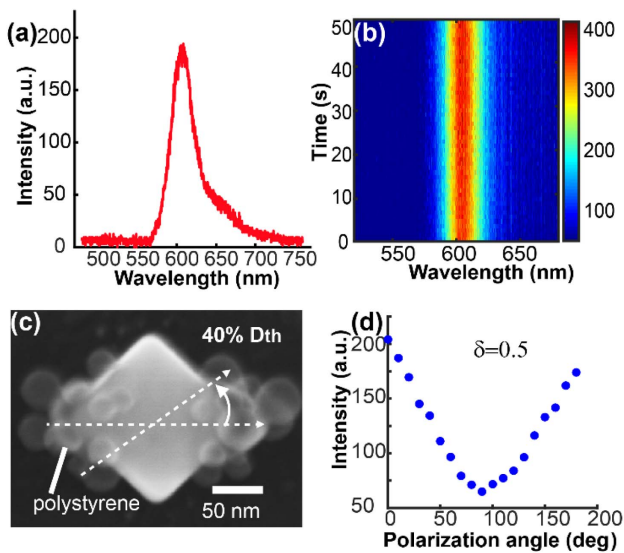


**Fig. 3.** (a) Fluorescence spectrum measured from the hybrid FPSs–GNC shown in Fig. 2(a) using polarized green laser of 532 nm wavelength for excitation. A 650/150 nm bandpass filter is used to separate the fluorescent signal from the incident excitation. (b) Spectrum time trace, collected for 50s. (c) Definition of the polarization angle for excitation. (d) Fluorescence intensity as a function of the angle of incident polarization defined in (c).

The fluorescence lifetime of the FPSs on the hybrid nanostructures, resulting from Step 2, was measured to study the influence of the polymer thickness and thus the mean value of the FPS–GNC distance. Figure 4(a) shows typical lifetime measurements. When the FPSs are directly attached to pure polymer dots without GNC [red curve in Fig. 4(a)], the lifetime is longer than it is when the FPSs are attached to the polymer lobes on the GNC, which is in agreement with what is expected; i.e., an increase of the radiative and nonradiative deactivation rates in the presence of the metal nanostructure. The lifetime decreases as the energy dose used for fabrication

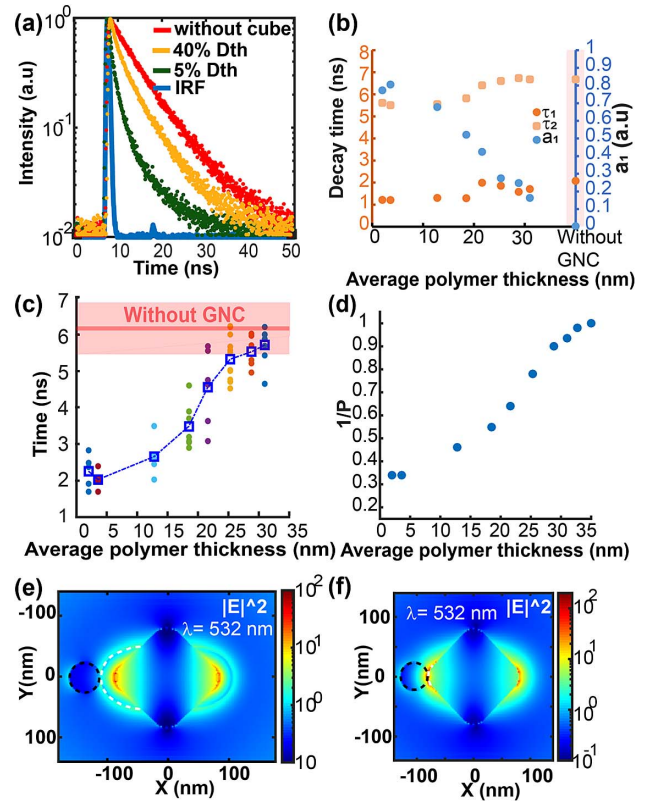


**Fig. 4.** (a) Lifetime measurement of FPSs attached on hybrid polymer-cube fabricated by a dose of 40% Dth (orange) and 5% Dth (green). (b) Double-exponential fitting results of the lifetime of FPSs: fast decay component  $\tau_1$ , slow decay component  $\tau_2$ , and the coefficient  $a_1$  of fast decay component change as the average polymer thickness varies. (c) Weighted average lifetimes of FPSs change along the average distance between the metal surface and FPSs increased by decreasing the incident dose used to fabricate the hybrid GNC-based nanostructures. Dots of the same color represent hybrid nanostructures made with the same excitation energy dose. The pink area represents the variation range of the fluorescence lifetime of FPSs attached on polymer dots in the absence of gold particles. (d) Simulated average Purcell factor ( $P$ ) of dipoles varies as the nano-polymer distribution changes by considering different incident energy doses and resulting average thicknesses. (e) and (f) Simulated field intensity (at  $Z = 25$  nm away from the bottom of the cube) of a hybrid FPS–GNC nanostructure fabricated individually using the energy dose of 40% Dth and 5% Dth. The excitation wavelength is set at 532 nm, and the incident light is polarized along  $X$ . The black dotted line depicts the FPS, and the white dotted line describes the contour of polymer.

decreases. The green curve (5% Dth) demonstrates a much shorter lifetime decay than the orange curve (40% Dth).

There are hundreds of molecules in each FPS ( $3.5 \times 10^2$  fluorescein equivalents per polystyrene sphere). In general, the overall decay of all the molecules can be fitted by a sum of exponential functions [42]; i.e.,

$$I_{\text{total}}(t) = \sum_{i=1}^N A_i \cdot \exp(-t/\tau_i), \quad (1)$$

where  $N$  is the number of dyes,  $I_{\text{total}}(t)$  is the normalized fluorescence intensity at time  $t$  from all the FPSs,  $A_i$  is the probability density function, and  $\sum_i^N A_i = 1$ . Parameter  $i$  can be viewed as a specific family of molecules that is characterized by lifetime  $\tau_i$ . The fluorescence lifetime of the FPSs without GNC can be very well fitted using a single-exponential function [see Fig. 14(a) in Appendix G], suggesting a single family of molecules, with a lifetime in the 6–7 ns range. With the presence of the GNC, the experimental data were fitted by one-exponential, double-exponential, and triple-exponential functions. An accurate fit was achieved with the double-exponential function, while the third exponential component has near-zero probability density [Figs. 14(b) and 14(c), in Appendix G]. Hence, the whole decay can be expressed as

$$I(t) = a_1 \exp\left(-\frac{t}{\tau_1}\right) + (1 - a_1) \exp\left(-\frac{t}{\tau_2}\right). \quad (2)$$

The double-exponential fitting results with different polymer thicknesses are shown in Fig. 4(b). Clearly, we observe a fast decay  $\tau_1$  that is contained in the 1–2 ns range and a slow decay  $\tau_2$  that is roughly stable within the 6–7 ns range. Considering the size of the FPS and keeping in mind that several FPSs are attached, we assign the fast decay  $\tau_1$  to the contribution of the Purcell effect undergone by the dye molecules, while the slow decay  $\tau_2$  is assigned to the emission of unaffected/less affected dye molecules, which is similar to the treatment in Ref. [43].  $\tau_1$  can be seen as the mean value of the fluorescence lifetimes [Eq. (1)] of the molecules that are sensitive to the GNC. Coefficient  $a_1$  stands for the weight of this fast decay component. It is associated with the proportion of molecules that undergo the Purcell effect. As shown in Fig. 4(b),  $a_1$  increases when the average polymer thickness decreases. This indicates an increase of the proportion of the dye molecules that are affected, in terms of the Purcell effect, by the presence of the GNC.

The weighted average lifetime [ $a_1\tau_1 + (1 - a_1)\tau_2$ ] is shown in Fig. 4(c). It is represented as a function of the average polymer thickness defined in Appendix E. To statistically assess the influence of the dose, between four and eight [corresponding to the different dots in Fig. 4(c)], hybrid nanostructures have been made for each given dose. Combining the SEM and AFM analysis before FPSs attachment (see Appendix E, Fig. 12), the estimated polymer 3D distribution and the average polymer thickness can be related to the levels of energy dose. Consequently, the change in the fluorescence lifetime of the FPSs can be presented as a function of the average polymer thickness, as shown in Fig. 4(c). This clearly statistically reveals a trend: the lifetime decreases as the average polymer thickness decreases and tends to a stable value  $\sim 2$  ns. Figure 4(d) shows

the corresponding simulated results through the inverse of the Purcell factor; i.e., the ratio of the de-excitation rate with and without the GNC. The fluorescence lifetime was calculated by placing dipoles at the center of the FPSs at the position corresponding to the polymer distribution, as observed by SEM and AFM (see Appendix E). Figures 4(c) and 4(d) reveal a consistent lifetime change trend, which confirms that the average polymer thickness is controlled by the incident energy dose used for fabrication of the hybrid nanosource, resulting in control of the FPS–GNC distance and the fluorescence lifetime of the FPSs. As a conclusion of this section, through fittings, it turns out that, while  $\tau_1$  and  $\tau_2$  remain relatively stable,  $a_1$  is very sensitive to the polymer thickness, resulting in significant sensitivity of the resulting averaged weighted lifetime [ $a_1\tau_1 + (1 - a_1)\tau_2$ ] that can be viewed as a “tunable barycenter” in the continuous sum of lifetimes in Eq. (1).

### C. Further Discussion about the Contributing Molecules within an FPS

From Figs. 4(c) and 4(d), a maximum Purcell factor can be estimated at 3.1 for the smallest polymer thickness, which is a rather low factor. Because of the size of an FPS, even if the polymer thickness is negligible, a large proportion of molecules within an FPS are still too far away from GNC, and the proportion of the unaffected/less affected molecules cannot go to zero. As a result,  $1 - a_1$  always  $> 0$ . This point is illustrated by Figs. 4(e) and 4(f) in terms of near-field excitation. Two hybrid nanosources were considered: one fabricated with a 40% Dth dose [Fig. 4(e)], polymer thickness of 21.6 nm, and the other fabricated with a 5% Dth [Fig. 4(f)], polymer thickness of 2 nm (see Appendix E, Table 1). For simplicity, both hybrid nanosources present a single FPS. The intensity map at  $Z = 25$  nm ( $\lambda = 532$  nm) was calculated by the finite-difference time-domain (FDTD) method using an incident  $X$ -polarized plane wave propagating along  $Z$ . The spatial distribution of the intensity reveals the two families of molecules in terms of excitation. In Fig. 4(e), there is a smaller proportion of dyes inside polystyrene sphere that are coupled to the localized field of the GNC (“close”). Even if this near-field map represents the excitation (rather than the de-excitation to the local density of states), it illustrates that the contribution of plasmon-coupled molecules to the average lifetime/Purcell factor of the whole system is weak; most of the molecules whose lifetimes play the main role in the whole system are unaffected by the GNC (“far”). In Fig. 4(f), a bigger proportion of dyes are coupled to the localized plasmonic near field and their contribution to the lifetime decrease becomes significant. This is consistent with the double exponential fitting results in Fig. 4(b). The discussions above can also explain why, when the polymer thickness decreases to the smallest, the weighted lifetime/average Purcell factor does not continue to decline, but tends to stabilize in Figs. 4(c) and 4(d).

### D. Use of Semiconductor Colloidal Quantum Dots as Nano-Emitters

To address the issue above, another approach was investigated. Semiconductor colloidal QDs were immobilized on a functionalized nanopolymer surface in the close vicinity of a single GNC. Compared to FPS, they can be considered as point-like

emitters. After Step 1 of fabrication, which is illustrated in Fig. 1(d), the hybrid GNC was immersed in a colloidal solution of negatively charged CdSe/ZnS red QDs (with carboxylic acid as reactive group, bought from Mesolight), with an emission wavelength at 623 nm and a diameter  $\approx 12$  nm [Figs. 8(c) and 8(d), Appendix B]. The obtained results, presented in Fig. 5(a), show a precise and selective attachment of QDs on the two corners of the GNC where the functionalized polymer was printed by the plasmon-induced polymerization: Figure 5(a) is the AFM image of a hybrid polymer/GNC/QDs obtained with a 40% Dth energy used for fabrication (Step 1). It clearly shows QDs attached at the surface of the integrated polymer lobes. More data with different energy doses can be found in Appendix C, Fig. 10.

Figure 5(b) shows a typical photoluminescence (PL) spectrum centered at  $\lambda = 620$  nm collected in the far field for 50 s (excitation at 405 nm). As for the FPS-based hybrid

sources, the active medium is anisotropic, making the sources sensitive to the incident polarization. Figure 5(c) shows the PL intensity as a function of the polarization direction of the excitation at 405 nm. Note that the definition of this direction is the same as for Fig. 3(c).

QDs generally have multi-exponential decay dynamics, which are due to their surface defects, surface ligands, inhomogeneities of ensemble sample, or other characteristics [44–46]. Unlike the situation with FPSs, the reference lifetime from QDs attached on the polymer dot without GNC nearby can be fitted well by double-exponential decay [Appendix G, Fig. 15(a)]. The short-time component and long-time component come from two different decay pathways [47]. Without GNC, these both lifetimes represent a reference that is intrinsic to the semiconducting nanocrystal.

With the presence of GNC, the decay of the QDs is influenced by the Purcell effect, depending on their relative positions to GNC. The lifetime of QDs can still be fitted by double exponential functions [Appendix G, Fig. 15(b)]. Then the normalized intensity can be presented as

$$I(t) = \alpha \exp(-t/\tau_\alpha) + (1 - \alpha) \exp(-t/\tau_\beta), \quad (3)$$

where  $\tau_\alpha$  is the fast decay,  $\tau_\beta$  is the slow decay, and  $\alpha$  describes the contribution of  $\tau_\alpha$ . Figure 5(d) shows a typical lifetime measurement of different hybrid nanosources fabricated with different energy doses ranging from 10% to 90% of Dth. From Fig. 5(d), the curves are fitted by double-exponential decay, using Eq. (3), and the fitting results are shown in Fig. 5(e).

The origin of this double-exponential decay is different from what it is in Eq. (2). In Eq. (3), it results from the intrinsic properties of the QDs [44–47] while it corresponds to two families of molecules in Eq. (2) (far and close molecules). Due to the small size of the QDs, all the QDs are affected in the same way by the presence of the GNC (Appendix E, Fig. 13). As a result, both lifetimes are sensitive to the polymer thickness, as shown in Fig. 5(e).

Figure 5(f) shows the weighted average lifetime  $[\alpha\tau_\alpha + (1 - \alpha)\tau_\beta]$  for different polymer thicknesses. Again, for each dose, many similar structures (from six to nine) were fabricated to get a statistical trend. From Figs. 5(d) and 5(f), it turns out that the weighted average lifetime decreases with the dose, as a result of the decrease of the average distance between quantum nano-emitters and GNC. Figure 5(e) shows the fitted values  $\tau_\alpha$ ,  $\tau_\beta$ , and  $\alpha$ , as a function of the average polymer thickness. Compared to Fig. 4(b), Fig. 5(e) reveals different features of interest. In Fig. 4(b), we saw that both decay components are almost stable, and  $a_1$  increases obviously as the polymer thickness decreases, mainly revealing an increase in the proportion of molecules that are influenced by the GNC and a displacement of the barycenter in Eq. (1). In Fig. 5(e), the components are both affected:  $\tau_\alpha$  and  $\tau_\beta$  decrease together as the average polymer thickness gets smaller. Note that it is actually impossible to keep  $\tau_\alpha$  and  $\tau_\beta$  stable, as shown in Fig. 15(c). Meanwhile, coefficient  $\alpha$  presents a weak increase (0.8 to 1), which is still tiny compared to the situation of an FPS-attached hybrid GNC; in Fig. 4(b),  $a_1$  varies from 0.9 to 0.1. There are two possible explanations. First,  $\alpha$  not only represents the intrinsic ratio between the two decay pathways but also includes a weak increase of the proportion of QDs influenced by GNC as the polymer

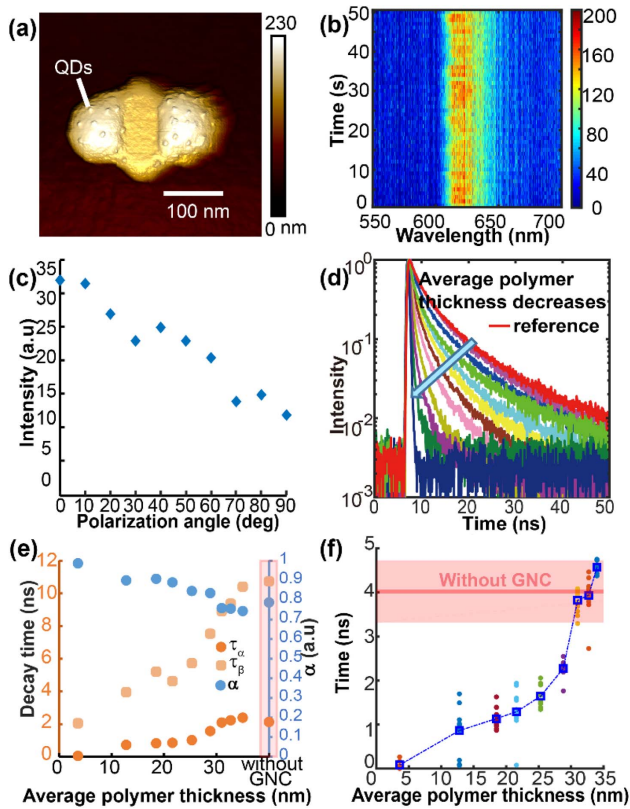


**Fig. 5.** Use of the smart polymer to couple spherical CdSe/ZnS quantum dots with gold nanocubes. (a) AFM image of a hybrid nanosource made with an energy dose of 40% Dth. Attached QDs that result from Step 2 of the fabrication are clearly visible. (b) The spectrum time trace, signal collected during continuous 50 s. (c) Polarization sensitivity of the hybrid nanosource. (d) Measured lifetime for different hybrid nanosources with different polymer thicknesses. The red curve represents a reference lifetime decay of QDs attached on a polymer dot without a GNC nearby. (e) Double-exponential fitting results: evolution of fast and slow decay components  $\tau_\alpha$ ,  $\tau_\beta$ , and coefficient  $\alpha$  of a fast component as a function of the average polymer thickness. (f) Weighted lifetime as a function of the average polymer thickness that depends on the fabrication condition (proportion percentage in Dth energy used for near-field photo polymerization in Step 1).

thickness decreases. Second, the short time component of QDs already plays the major role in free space, and a change in it cannot be distinguished as a change in the long-time component because of the resolution limitation of the setup. For FPSs, the variation in the weighted average lifetimes is instead mainly due to  $a_1$ . In addition, according to Fig. 5(f), quite different from Fig. 4(c), the maximum Purcell factor in the situation of attached QDs can get larger than 10. This is because, due to their small size, at a small polymer thickness, QDs may be strongly affected by the Purcell effect, and no QDs can escape from the influence of a GNC.

#### 4. CONCLUSION

The use of smart photopolymers has led to new kinds of plasmonic hybrid nanosources where different types of nanoemitters can be integrated on demand at predesigned sites of the metal nanostructures. The cleverness of the polymer makes possible the selection of the site through local plasmon excitation that results in a 3D spatial memory. In particular, it is possible to control the average distance between the metal nanostructure and the emitter to be attached. This latter is recognized by the polymer through charge affinity, leading to its selective controlled attachment.

Compared to Ref. [33], many advantages can be stressed. First, we can achieve a wider variety of emitters. While the integration of emitters within the initial acrylate-type liquid formulation is delicate in terms of phase separation and photochemical effects [48], the new approach reported here allows any negatively charged emitters or particles to attach to the surface of polymer lobes with the help of electrostatic forces. In the future, we believe this approach will open up many routes. For example, even negatively charged nanodiamonds permitting single photon emission [49] could be selectively attached. Second, the main novelty lies in the fact that we still have the advantages of our previous method, which can place emitters close to plasmonic structures with anisotropic distribution, and further improves it with more possibilities. By placing emitters on the surface of the polymer, the thickness of polymer is also the distance between the emitters and the plasmonic

particles, instead of letting the emitters be randomly dispersed inside the whole volume of the polymer lobes. Controlling this distance has led to actual lifetime engineering. To comment further on this point, let us consider the spherical coordinates  $(\phi, \theta, \rho)$  of the emitter to be localized. We can control  $\phi, \theta$  using the method introduced in Ref. [33]. We now control  $\rho$  with our new functionalized photopolymer approach.

Finally, the surface attachment method is likely to avoid a bad influence from the laser during polymerization, which may damage the emitters or introduce other effects such as light force and two-photon absorption, which are currently being studied by our team.

This approach will be used to fabricate single-photon hybrid nanosources [33] and precisely integrate different kinds of QDs through a multistep process [34] that we believe will open new avenues for advanced integrated nanosources based on weak and strong coupling, among which are multicolor nanolasers [34,50] that may be controlled by light polarization. In addition, as we demonstrated in Ref. [33], through the concept of a polarization-dependent spatial overlap integral (overlap between the exciting near field and the emitters), a tunable emitter selection is possible by rotating the incident polarization. However, in Ref. [33], the excitation was in the blue, which is suitable for emitter excitation but not plasmon excitation. By integrating emitters that efficiently get excited at a 780 nm wavelength through either one or two-photon absorption, we would take advantage of the plasmonic hot spot to both integrate and excite them in the future.

#### APPENDIX A: PROCESS OF FABRICATION

The separation distance between GNCs is controlled to be larger than 500 nm by adjusting the concentration of GNCs in the solution, to avoid the influence from each other in the following experiments, including two-photon polymerization and emission measurement.

Figure 6 illustrates the steps to prepare the hybrid FPS-attached cubes. Figure 7 gives the optical setup used to do two-photon polymerization on each single GNC. The positions of the focused laser spot and GNCs are observed by a

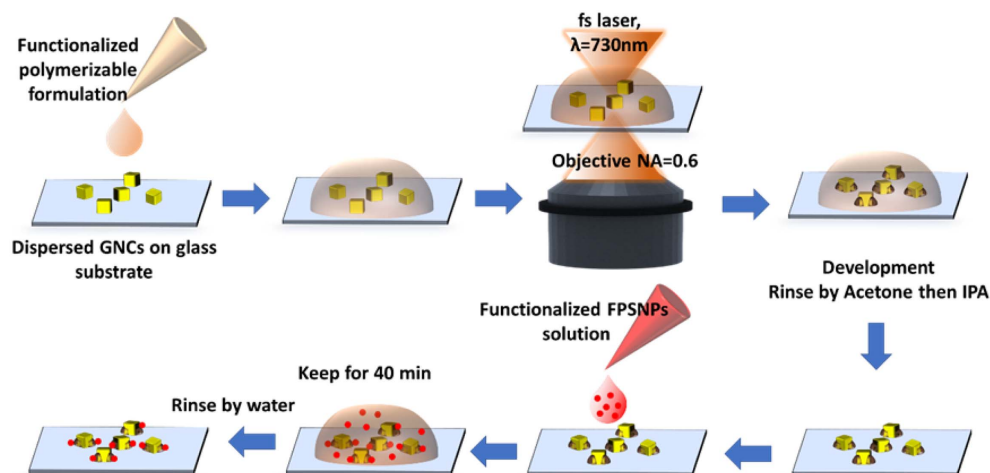
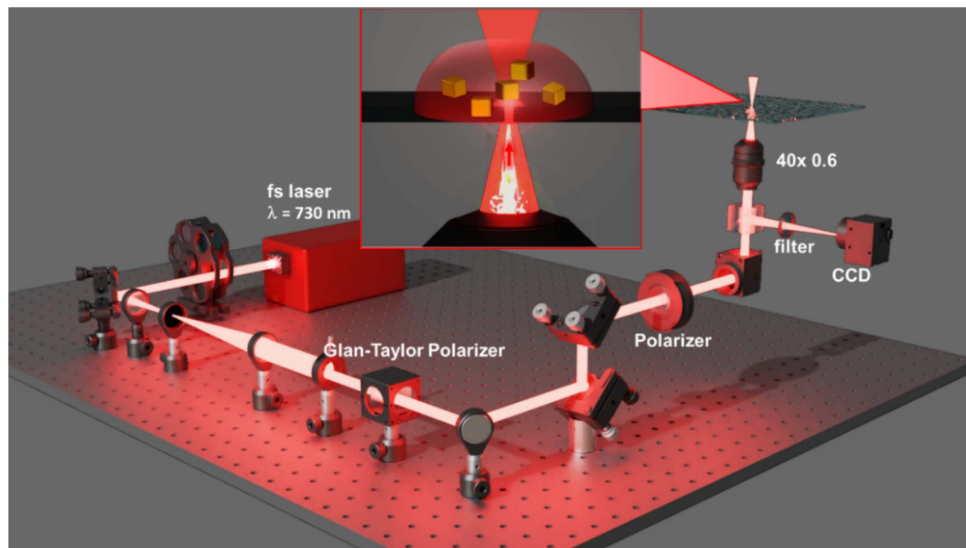


Fig. 6. The process steps for fabricating hybrid FPS-attached cubes (FPS: fluorescent polystyrene sphere).



**Fig. 7.** Optical configuration to carry out two-photon polymerization.

CCD camera, which makes it possible to aim the laser spot at each isolated GNC.

The GNCs are dispersed on a glass substrate with a separation distance between each other that is larger than 500 nm. A drop of the functionalized photosensitive formulation is then deposited on the pre-identified GNCs sample. Each GNC of a

consistent size and good shape is exposed one by one using a focused femtosecond laser of 730 nm by an objective lens (NA = 0.6), as shown in Fig. 7. During polymerization, the exposure time is kept at 1/15 s. The exposure laser energy dose is set below the polymerization threshold and is defined as the percentage of threshold dose (typical incident dose

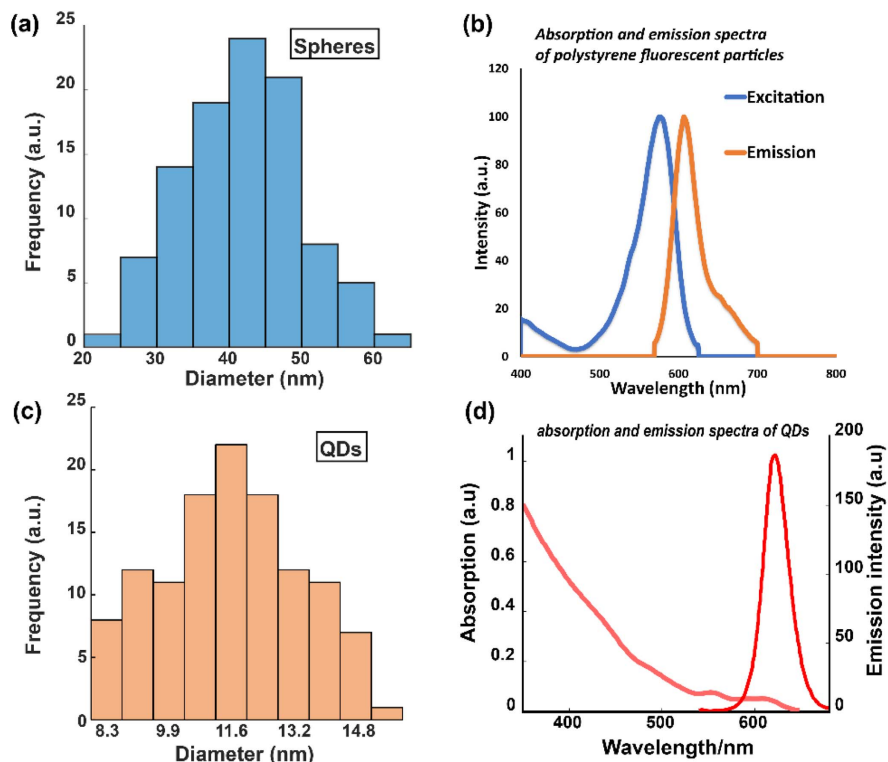


**Fig. 8.** (a) Diameter distribution histogram of the fluorescent polystyrene spheres. (b) Excitation and emission spectra of polystyrene spheres measured separately by UV-visible Cary 100 spectrometer and fluorescence spectrophotometer. (c) Diameter distribution histogram of the QDs. The QDs are deposited on a glass substrate and then, after coating of a conducting layer, the QD sizes are measured under an SEM. Due to the existence of the conductive layer, the size of the measured QD is several nanometers larger than the real size of the QDs. (d) The absorption and emission spectra of the red QDs in toluene.

$D_{in} = 40\%$  Dth). The polarization direction of curing laser is along the diagonal of the GNCs.

### APPENDIX B: SIZE OF POLYSTYRENE FLUORESCENT PARTICLES AND QUANTUM DOTS

From Fig. 8(a), the average diameter of this kind of fluorescent polystyrene sphere is around 42.5 nm. Different sizes of polystyrene spheres will change the related distance between their molecules containing fluorescent dye and the GNC, which will lead to errors in the fluorescence lifetime measurement. When the number of attached polystyrene spheres is relatively large, since the measured fluorescence lifetime is a statistical average, the influence of the size difference of polystyrene spheres on the result can be ignored. However, when the hybrid GNC is fabricated by a low dose, the number of attached polystyrene spheres is limited, and the size difference of the fluorescent spheres becomes non-negligible. That can explain why the measured lifetime in the situation of a smallest average thickness is longer than in the second smallest situation in Fig. 4(b).

These Thermo Fisher Scientific fluorescent FluoSpheres beads have an average diameter around 42 nm with the dyes filling the full volume of the beads, and they contain 3500 fluorescein equivalents per microsphere, according to the Thermo Fisher Scientific handbook.

### APPENDIX C: MORE EXAMPLES OF HYBRID NANOCUBES

The number of FPSs/QDs attached on the polymer lobes is related to the size of the functionalized polymer. The dose used for fabrication of the hybrid structures affects the volume of polymer and then, determines the number of attached emitters, which is demonstrated by Figs. 9 and 10.

### APPENDIX D: POLARIZATION SENSITIVITY OF THE EMISSION INTENSITY

Figure 11 illustrates the polarization sensitivity of our hybrid-FPSs-GNC with two other examples of hybrid plasmonic nanosources. The polarization sensitivity  $\delta$ , which is defined as the ratio of the difference between the maximum light intensity and the minimum light intensity to their sum, keeps stable. This proves the repeatability of our method again.

### APPENDIX E: 3D POLYMER CHARACTERIZATION AND DEFINITION OF THE AVERAGE POLYMER THICKNESS

From SEM and AFM analysis before emitter attachment (Fig. 12), it is possible to define the average distance between the emitters and the gold nanocube (Fig. 13). For a  $Z_i$  slice, if the polymer thickness in the third quadrant is sampled at

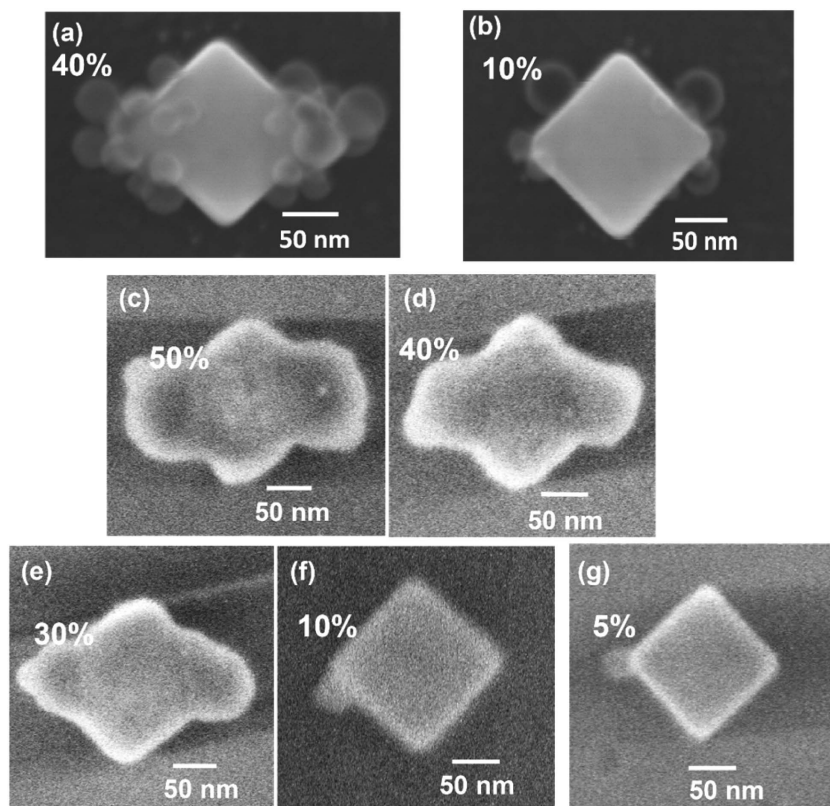


**Fig. 9.** More examples of hybrid FPS-attached GNCs. (a), (b) SEM images of the hybrid FPS-attached nanocubes fabricated using 40% Dth and 10% Dth, and the residence time of the FPS solution is 40 min. A 10 kV voltage is used for SEM observation. (c)–(g) FPS-attached nanocubes fabricated separately using 50% Dth, 40% Dth, 30% Dth, 10% Dth, and 5% Dth. The immersion time of the sample in the FPS solution is decreased to 10 min. A 1 kV voltage is used for SEM observation.

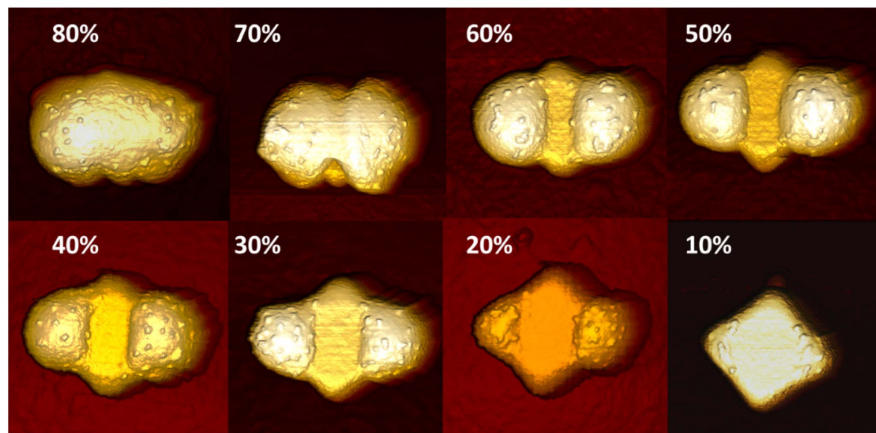


**Fig. 10.** AFM images of some hybrid GNCs with attached QDs, fabricated using incident doses from 80% decreasing to 10% of Dth (Step 1).

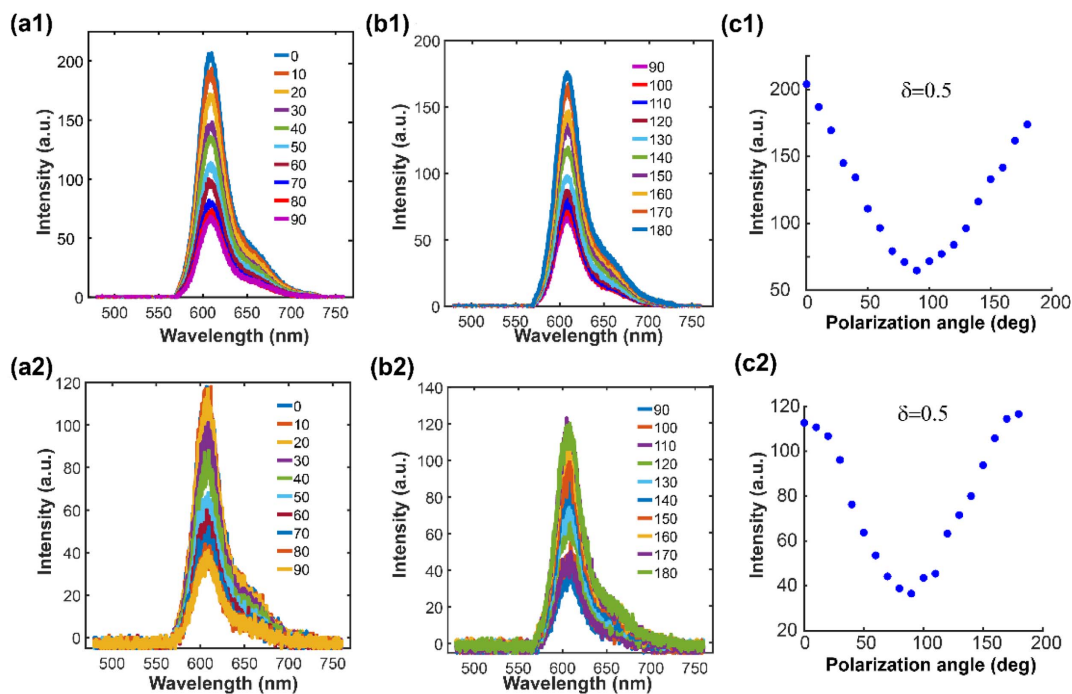


**Fig. 11.** Emission spectra from two hybrid FPS-attached GNCs fabricated using same parameters, and their exposure dose is 40% Dth. (a1) and (b1) The emission spectra from the first hybrid FPS-attached GNC when the polarization angle of the laser used for the excitation varies separately from 0 deg to 90 deg and 90 deg to 180 deg. (c1) The emission peak intensity changing trend. (a2), (b2), and (c2) The results from the second hybrid FPS-attached GNC.

30-degree intervals, which is shown in Fig. 13(b), three polymer thicknesses— $l_1$ ,  $l_2$ , and  $l_3$ —are obtained. Then, the average polymer thickness on a  $Z_i$  slice is  $(l_1 + l_2 + l_3)/3$ . For each  $Z_i$  slice, if you keep sampling at 30-degree intervals, the number of  $l$  obtained will vary with a change in the polymer distribution of each slice. Finally, the average of all obtained  $l$  is taken as the average polymer thickness.

## APPENDIX F: FLUORESCENCE SIGNAL AND LIFETIME MEASUREMENT

### 1. Optical Setup

For fluorescence intensity measurement, the FPSs-attached hybrid plasmonic nanosource is excited using 532 nm (CW laser,

OBIS 532 nm) focused by an objective lens (40 $\times$ , NA = 0.6). The fluorescence signal is collected by the same objective and, after filtering by a bandpass filter (FF01-650/150-25, Semrock), it is analyzed by a spectrometer. A half-wave plate is used to change the polarization direction of the linearly polarized incident beam. After each polarization rotation, one uses another polarizer to check the polarization direction. We also check the laser output light power to ensure that the power reaching the sample surface remains the same whatever the polarization direction (detected before objective lens, laser power is set to 10  $\mu$ W). For lifetime measurement, we use a pulsed laser (Picoquant D-TA-530B) connected with an extra driver box (PDL 800-B), whose repetition frequency is set at

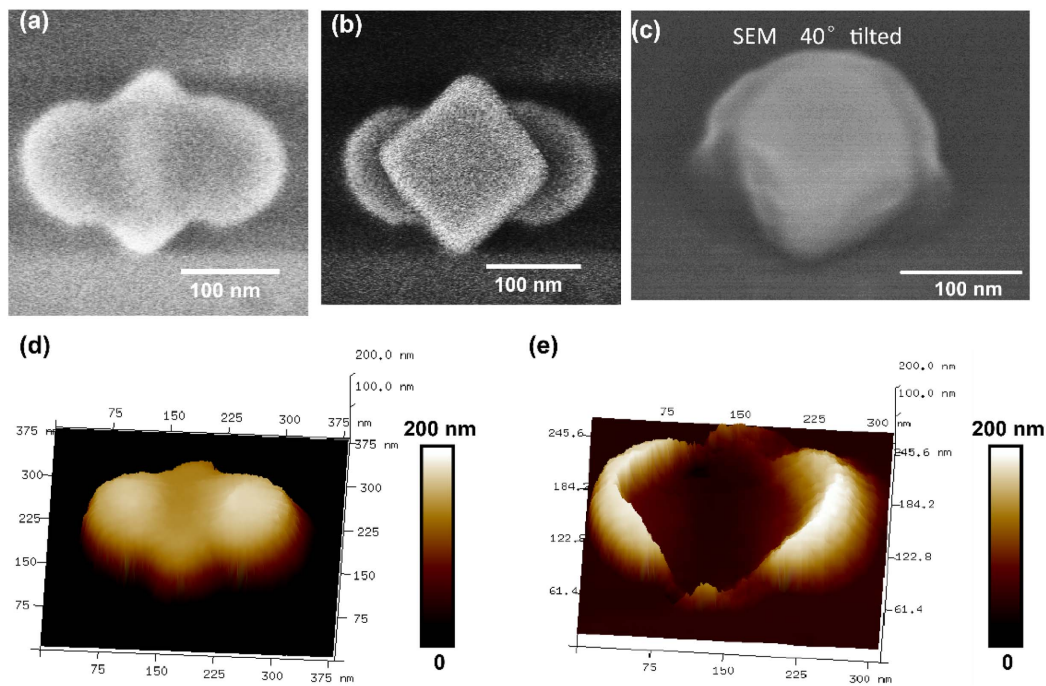


**Fig. 12.** (a) SEM image of a hybrid nanocube without attaching any QDs/polystyrene spheres (fabricated using 50% Dth). (b) Mixed image, the original SEM image of the cube before exposure is superimposed to (a). (c) 40-degree tilted SEM image. (d) 3D height image measured by AFM of the same hybrid nanocube as (a). (e) 3D height image subtracted by the original cube's height profile from (c), demonstrating the 3D polymer distribution.

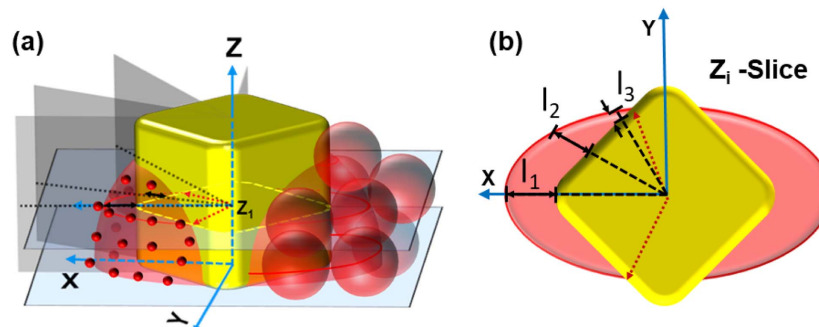


**Fig. 13.** Average polymer thickness definition and assessment. (a) The whole hybrid cube-polymer structure is cut in the  $Z$  direction to get 20 slices of the cross-section. For each  $Z$  slice, a quadrant is sliced into  $N$  parts on average according to angle, and the intersection of the corresponding rays and the polymer profile is averaged to obtain the average elongation of the polymer under this  $Z$  slice. Finally, the polymer thickness of all slices in the  $Z$  direction is averaged to get the average polymer thickness. (b) The polymer elongations ( $l_1$ ,  $l_2$ ,  $l_3$ ) obtained by the three tangents when a quadrant is divided into three sections in the  $Z_1$ -slice, and then the average value of the three elongation rates of the polymer thickness of this slice.

10 MHz. The laser beam is focused onto the sample by an objective lens (100 $\times$ , NA = 0.95). The laser power detected before the objective lens is about 0.5  $\mu$ W. Fluorescence from the hybrid nanosource is collected by reflection, and then after passing through a band-pass filter (FF01-650/150-25), light is collected by an optical fiber and directed towards an avalanche photodiode (APD, Picoquant PMA-182). The signal is sent to the stand-alone TCSPC module (PicoHarp-300, PicoQuant), which is linked to the laser driver.

## 2. Purcell Factor Simulation

The Purcell factor is calculated by FDTD. For each incident light dose, the corresponding 3D polymer is constructed as

**Table 1.** Calculated Average Polymer Thickness Using Different Percentages of Dth Doses

Percentage of Dth (%)	Average Polymer Thickness (nm)
5	2
10	3.6
20	12.8
30	18.5
40	21.6
50	25.3
60	28.8
70	31.0
80	32.7
90	34

a model with a refractive index of 1.5 and the diameter of the polystyrene sphere is set to 50 nm. For each case, the hybrid polymer cube is cut into  $N$  slices in the  $Z$  direction, and each  $Z_i$  slice has a specific polymer contour at the  $Z$  position, as shown in Fig. 13. The FPSs are distributed along the contour of the polymer. To calculate, we only chose several FPSs along the contour at  $Z_i$ . For each nanosphere, we first calculated the Purcell factor of the ideal dipole at the center of the nanosphere, and then finally averaged these results to obtain the average Purcell factor of this  $Z$  slice by

$$PF_i = \frac{1}{N_i} \sum_{k=1}^{N_i} PF_k, \quad (\text{F1})$$

where  $N_i$  is the sampling number of FPSs on a  $Z_i$  slice.

The fluorescent nanoparticles (FPSs) are assumed uniformly distributed on the surface of polymer. Then, for each  $Z_i$  slice, the number of attached FSNPs depends on the length of the polymer contour line:

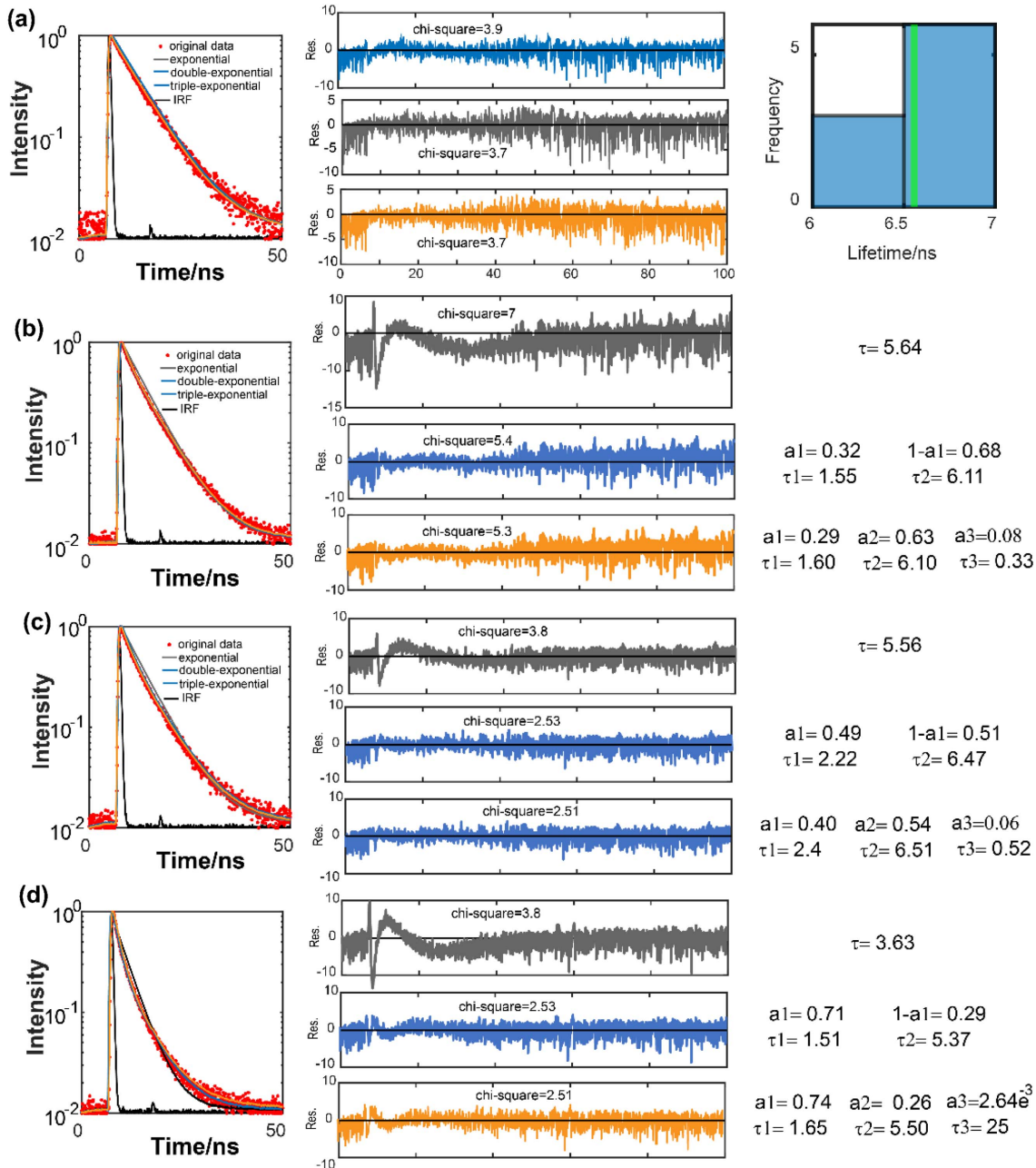


**Fig. 14.** (a) First row shows an example of the lifetime from FPSs attached on a pure polymer dot without GNC nearby. Three kinds of fittings are used here: single-exponential fitting (gray line), double-exponential fitting (blue line), and triple-exponential fitting (orange line). The fitting results show that the single-exponential function can already achieve a good fitting result. The far-right image shows the histogram of the FPSs' lifetime under a single-exponential fitting, and the green line represents the average value. For comparison, (b)–(d) show three examples of the lifetime from FPSs attached on the polymer lobes of a GNC.

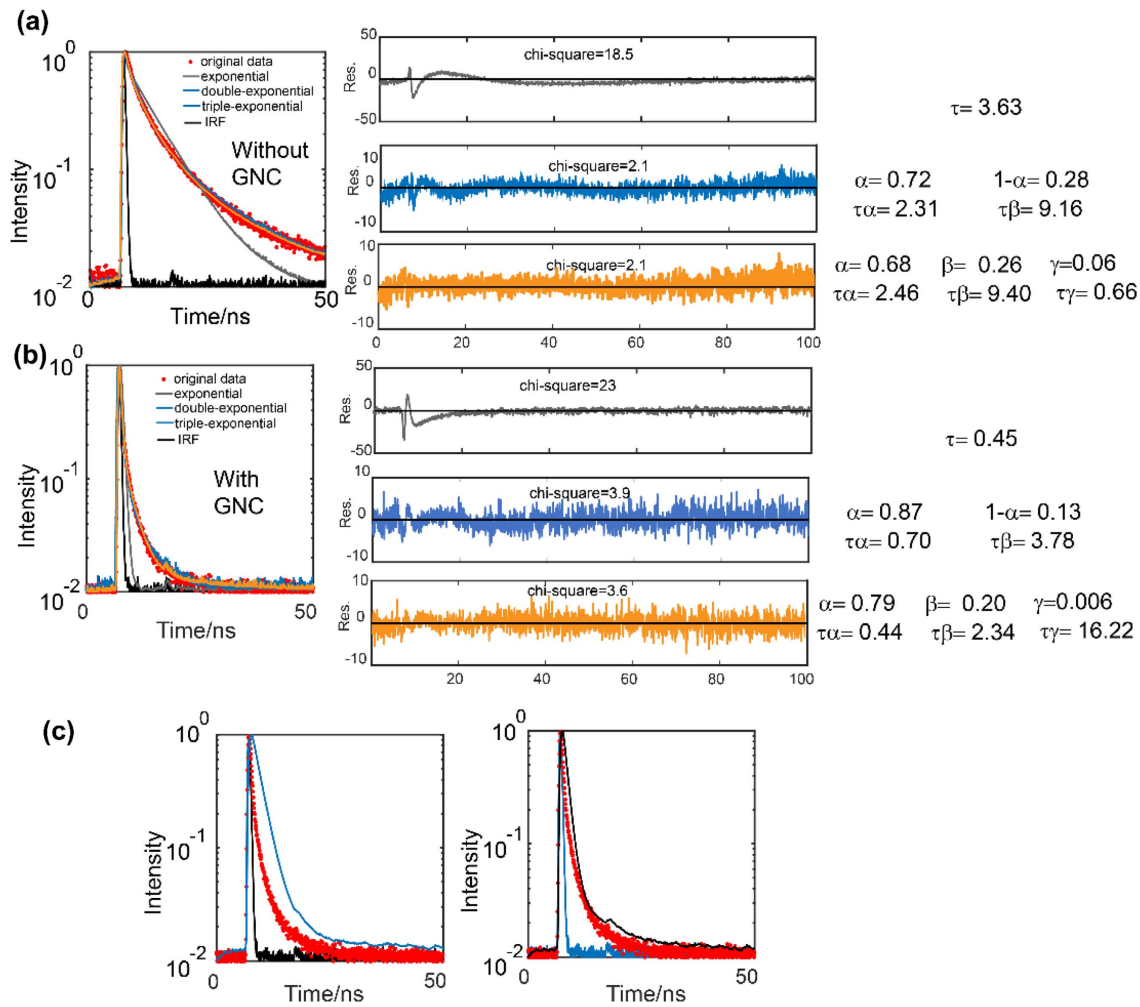


**Fig. 15.** Example of the lifetime from QDs attached on pure polymer dot (a) without a GNC nearby and (b) with a GNC nearby. A single-exponential function is not enough to get a good fitting result while a double- or triple-exponential function can get a better fit. (c) Two failed attempts, by limiting the value range of  $\tau_a$  (2–3),  $\tau_\beta$  (9–10) and  $\tau_\alpha$  (1–3),  $\tau_\beta$  (8–10) to attempt to use a similar  $\tau_a$ ,  $\tau_\beta$  in (a) to fit the decay curve.

$$PF_{\text{total}} = \left( \sum_{i=1}^{i=N} C_i \cdot PF_i \right) / \left( \sum_{i=1}^{i=N} C_i \right), \quad (\text{F2})$$

where  $C_i$  is the length of polymer contour line of a  $Z_i$  slice, and  $N$  is the number of slices in the  $Z$  direction.

In this way, the obtained  $PF_{\text{total}}$  works as the average Purcell factor in the case of a hybrid FPS-attached polymer cube fabricated by a certain dose.

For example, for 20% Dth, the polymer volume is cut into two slices in the  $Z$  direction. For slice 1, three positions of fluorescent spheres are calculated. For every position, we calculated the Purcell factor of an orientation-averaged dipole placed in the center of the sphere. And the boundary length of the polymer of this  $Z_1$  slice is around 48.7 nm. For the  $Z_2$ -slice, because the boundary length of polymer is much smaller than diameter of the sphere, we only calculate the Purcell factor at one position. Finally, an average Purcell factor  $\sim 2.17$  was obtained according to Eq. (F2).

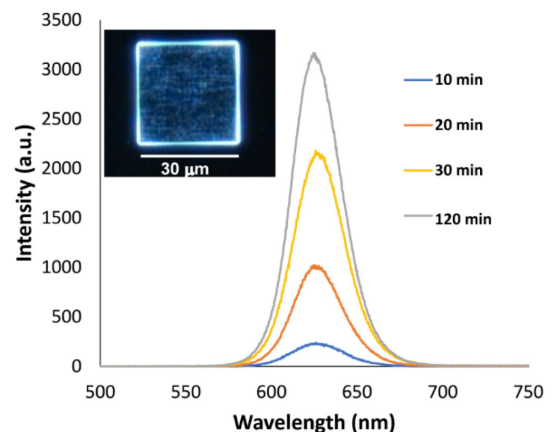


**Fig. 16.** Fluorescence intensity from QDs attached on 2D flat functionalized polymer structure (see inset) with respect to the immersion time (min). The excitation laser is at 405 nm with a power of 2  $\mu\text{m}$ , and the collection time is kept at 0.1 s. The left top small image (inset) is the dark-field image of the 2D flat polymer square.

## APPENDIX G: MULTI-EXPONENTIAL DECAY FITTING OF THE LIFETIME OF FPS AND QD IN FREE SPACE

The lifetimes of the FPSs/QDs on the hybrid GNC have been fitted by three kinds of ways: single-exponential fitting (gray line), double-exponential fitting (blue line), and triple-exponential fitting. The results shown in Fig. 14 prove that double-exponential fitting is enough for the lifetime of FPSs that are attached on the hybrid nanocube because the third component has an ignorable coefficient when they are fitted by triple-exponential function. Figure 15 illustrates that in the case of QDs, there is no obvious difference between double-exponential fitting and triple-exponential fitting. Double-exponential fitting is thus enough for presenting the time decay behavior of QDs photoluminescence.

## APPENDIX H: NUMBER OF ATTACHED EMITTERS

In Ref. [36], the original principle of this chemically attached method has been described. In this article, gold nanoparticles (diameter  $\sim 50$  nm) were attached to the smart photopolymer. The control of the surface density (and thus the number) of gold nanoparticles has already been studied. The gold nanoparticles have the same size as the fluorescent spheres used in our current manuscript. We expect that their density changes with the immersion time following the same law.

As far as the QDs are concerned, Fig. 16 shows the fluorescence intensity from QDs attached on a micrometer-sized functionalized flat polymer structure. Different immersion times were used. Considering the fixed size of the polymer area, Fig. 16 clearly shows that the intensity (and thus the related number of attached QDs) strongly depends on the immersion time.

**Funding.** FEDER; The Région Grand Est; Université de Technologie de Troyes; École Universitaire de Recherche (ANR-18-EURE-0013).

**Acknowledgment.** Dandan Ge gratefully thanks the China Scholarship Council (CSC) for funding support. Fabrication and characterization were mostly done thanks to the Nano'Mat platform, supported by the Ministère de l'Enseignement Supérieur et de la Recherche, the Région Grand Est (Pronano project), the Conseil Général de l'Aube, and FEDER (Pronano and Q-LED projects) funds from the European Community. This work has been made within the framework of the Graduate School NANO-PHOT (École Universitaire de Recherche). The paper was written through contributions from all the authors. All the authors have approved the final version of the paper.

**Disclosures.** The authors declare no conflicts of interest.

**Data Availability.** Data underlying the results presented in this paper are not publicly available at this time but may be obtained from the authors upon reasonable request.

## REFERENCES

1. F. Vetrone, R. Naccache, A. Zamarrón, A. J. de la Fuente, F. Sanz-Rodríguez, L. M. Maestro, E. M. Rodríguez, D. Jaque, J. G. Sole, and J. A. Capobianco, "Temperature sensing using fluorescent nanothermometers," *ACS Nano* **4**, 3254–3258 (2010).
2. J.-H. Kim, S. Aghaeimeibodi, C. J. K. Richardson, R. P. Leavitt, D. Englund, and E. Waks, "Hybrid integration of solid-state quantum emitters on a silicon photonic chip," *Nano Lett.* **17**, 7394–7400 (2017).
3. X. Feng, Y. Li, X. He, H. Liu, Z. Zhao, R. T. K. Kwok, M. R. J. Elsegood, J. W. Y. Lam, and B. Z. Tang, "A substitution-dependent light-up fluorescence probe for selectively detecting Fe<sup>3+</sup> ions and its cell imaging application," *Adv. Funct. Mater.* **28**, 1802833 (2018).
4. T. B. Hoang, G. M. Akselrod, C. Argyropoulos, J. Huang, D. R. Smith, and M. H. Mikkelsen, "Ultrafast spontaneous emission source using plasmonic nanoantennas," *Nat. Commun.* **6**, 7788 (2015).
5. G. M. Akselrod, C. Argyropoulos, T. B. Hoang, C. Ciraci, C. Fang, J. Huang, D. R. Smith, and M. H. Mikkelsen, "Probing the mechanisms of large Purcell enhancement in plasmonic nanoantennas," *Nat. Photonics* **8**, 835–840 (2014).
6. Y. Luo, E. D. Ahmadi, K. Shayan, Y. Ma, K. S. Mistry, C. Zhang, J. Hone, J. L. Blackburn, and S. Strauf, "Purcell-enhanced quantum yield from carbon nanotube excitons coupled to plasmonic nanocavities," *Nat. Commun.* **8**, 1413 (2017).
7. H. Aouani, O. Mahboub, E. Devaux, H. Rigneault, T. W. Ebbesen, and J. Wenger, "Plasmonic antennas for directional sorting of fluorescence emission," *Nano Lett.* **11**, 2400–2406 (2011).
8. P. Anger, P. Bharadwaj, and L. Novotny, "Enhancement and quenching of single-molecule fluorescence," *Phys. Rev. Lett.* **96**, 113002 (2006).
9. H. Leng, B. Szychowski, M.-C. Daniel, and M. Pelton, "Strong coupling and induced transparency at room temperature with single quantum dots and gap plasmons," *Nat. Commun.* **9**, 4012 (2018).
10. A. Kinkhabwala, Z. Yu, S. Fan, Y. Avlasevich, K. Müllen, and W. E. Moerner, "Large single-molecule fluorescence enhancements produced by a bowtie nanoantenna," *Nat. Photonics* **3**, 654–657 (2009).
11. S. Khatua, P. M. R. Paulo, H. Yuan, A. Gupta, P. Zijlstra, and M. Orrit, "Resonant plasmonic enhancement of single-molecule fluorescence by individual gold nanorods," *ACS Nano* **8**, 4440–4449 (2014).
12. K. J. Russell, T.-L. Liu, S. Cui, and E. L. Hu, "Large spontaneous emission enhancement in plasmonic nanocavities," *Nat. Photonics* **6**, 459–462 (2012).
13. R. Chikkaraddy, B. de Nijs, F. Benz, S. J. Barrow, O. A. Scherman, E. Rosta, A. Demetriadou, P. Fox, O. Hess, and J. J. Baumberg, "Single-molecule strong coupling at room temperature in plasmonic nanocavities," *Nature* **535**, 127–130 (2016).
14. T. B. Hoang, G. M. Akselrod, and M. H. Mikkelsen, "Ultrafast room-temperature single photon emission from quantum dots coupled to plasmonic nanocavities," *Nano Lett.* **16**, 270–275 (2016).
15. T. Ming, L. Zhao, Z. Yang, H. Chen, L. Sun, J. Wang, and C. Yan, "Strong polarization dependence of plasmon-enhanced fluorescence on single gold nanorods," *Nano Lett.* **9**, 3896–3903 (2009).
16. S.-Y. Liu, L. Huang, J.-F. Li, C. Wang, Q. Li, H.-X. Xu, H.-L. Guo, Z.-M. Meng, Z. Shi, and Z.-Y. Li, "Simultaneous excitation and emission enhancement of fluorescence assisted by double plasmon modes of gold nanorods," *J. Phys. Chem. C* **117**, 10636–10642 (2013).
17. A. W. Schell, P. Engel, J. F. M. Werra, C. Wolff, K. Busch, and O. Benson, "Scanning single quantum emitter fluorescence lifetime imaging: quantitative analysis of the local density of photonic states," *Nano Lett.* **14**, 2623–2627 (2014).
18. H. Groß, J. M. Hamm, T. Tufarelli, O. Hess, and B. Hecht, "Near-field strong coupling of single quantum dots," *Sci. Adv.* **4**, eaar4906 (2018).
19. M. P. Busson, B. Rolly, B. Stout, N. Bonod, and S. Bidault, "Accelerated single photon emission from dye molecule-driven nanoantennas assembled on DNA," *Nat. Commun.* **3**, 962 (2012).
20. X. Lan, X. Zhou, L. A. McCarthy, A. O. Govorov, Y. Liu, and S. Link, "DNA-enabled chiral gold nanoparticle–chromophore hybrid structure with resonant plasmon–exciton coupling gives unusual and strong circular dichroism," *J. Am. Chem. Soc.* **141**, 19336–19341 (2019).

21. A. T. M. Yeşilyurt and J.-S. Huang, "Emission manipulation by DNA origami-assisted plasmonic nanoantennas," *Adv. Opt. Mater.* **9**, 2100848 (2021).
22. M. Loretan, I. Domljanovic, M. Lakatos, C. Rüegg, and G. P. Acuna, "DNA origami as emerging technology for the engineering of fluorescent and plasmonic-based biosensors," *Materials* **13**, 2185 (2020).
23. K. Hübner, M. Pilo-Pais, F. Selbach, T. Liedl, P. Tinnefeld, F. D. Stefani, and G. P. Acuna, "Directing single-molecule emission with DNA origami-assembled optical antennas," *Nano Lett.* **19**, 6629–6634 (2019).
24. R. Chikkaraddy, V. A. Turek, N. Kongsuwan, F. Benz, C. Carnegie, T. van de Goor, B. de Nijs, A. Demetriadou, O. Hess, U. F. Keyser, and J. J. Baumberg, "Mapping nanoscale hotspots with single-molecule emitters assembled into plasmonic nanocavities using DNA origami," *Nano Lett.* **18**, 405–411 (2018).
25. H. Zhang, M. Li, K. Wang, Y. Tian, J.-S. Chen, K. T. Fontaine, D. DiMarzio, M. Liu, M. Cotlet, and O. Gang, "Polarized single-particle quantum dot emitters through programmable cluster assembly," *ACS Nano* **14**, 1369–1378 (2020).
26. G. P. Acuna, F. M. Möller, P. Holzmeister, S. Beater, B. Lalkens, and P. Tinnefeld, "Fluorescence enhancement at docking sites of DNA-directed self-assembled nanoantennas," *Science* **338**, 506–510 (2012).
27. J. Heintz, N. Markešević, E. Y. Gayet, N. Bonod, and S. Bidault, "Few-molecule strong coupling with dimers of plasmonic nanoparticles assembled on DNA," *ACS Nano* **15**, 14732–14743 (2021).
28. C. Shen, X. Lan, X. Lu, T. A. Meyer, W. Ni, Y. Ke, and Q. Wang, "Site-specific surface functionalization of gold nanorods using DNA origami clamps," *J. Am. Chem. Soc.* **138**, 1764–1767 (2016).
29. F. Wang, S. Cheng, Z. Bao, and J. Wang, "Anisotropic overgrowth of metal heterostructures induced by a site-selective silica coating," *Adv. Opt. Mater.* **52**, 10344–10348 (2013).
30. I. Tijunelyte, I. Kherbouche, S. Gam-Derouich, M. Nguyen, N. Lidgi-Guigui, M. L. de la Chapelle, A. Lamouri, G. Lévi, J. Aubard, A. Chevillot-Biraud, C. Mangeney, and N. Felidj, "Multi-functionalization of lithographically designed gold nanodisks by plasmon-mediated reduction of aryl diazonium salts," *Nanoscale Horiz.* **3**, 53–57 (2017).
31. V.-Q. Nguyen, Y. Ai, P. Martin, and J.-C. Lacroix, "Plasmon-induced nanolocalized reduction of diazonium salts," *ACS Omega* **2**, 1947–1955 (2017).
32. P. Zijlstra, P. M. R. Paulo, K. Yu, Q.-H. Xu, and M. Orrit, "Chemical interface damping in single gold nanorods and its near elimination by tip-specific functionalization," *Angew. Chem. Int. Ed.* **124**, 8477–8480 (2012).
33. D. Ge, S. Marguet, A. Issa, S. Jradi, T. H. Nguyen, M. Nahra, J. Béal, R. Deturche, H. Chen, S. Blaize, J. Plain, C. Fiorini, L. Douillard, O. Soppera, X. Q. Dinh, C. Dang, X. Yang, T. Xu, B. Wei, X. W. Sun, C. Couteau, and R. Bachelot, "Hybrid plasmonic nano-emitters with controlled single quantum emitter positioning on the local excitation field," *Nat. Commun.* **11**, 3414 (2020).
34. X. Zhou, J. Wenger, F. N. Viscomi, L. Le Cunff, J. Béal, S. Kochtcheev, X. Yang, G. P. Wiederrecht, G. C. des Francs, A. S. Bisht, S. Jradi, R. Caputo, H. V. Demir, R. D. Schaller, J. Plain, A. Vial, X. W. Sun, and R. Bachelot, "Two-color single hybrid plasmonic nanoemitters with real time switchable dominant emission wavelength," *Nano Lett.* **15**, 7458–7466 (2015).
35. S. Mitiche, S. Marguet, F. Charra, and L. Douillard, "Near-field localization of single Au cubes: a group theory description," *J. Phys. Chem. C* **121**, 4517–4523 (2017).
36. A. Issa, I. Izquierdo, M. Merheb, D. Ge, A. Broussier, N. Ghabri, S. Marguet, C. Couteau, R. Bachelot, and S. Jradi, "One strategy for nanoparticle assembly onto 1D, 2D, and 3D polymer micro and nanostructures," *ACS Appl. Mater. Interfaces* **13**, 41846–41856 (2021).
37. J. de Torres, P. Ferrand, G. C. des Francs, and J. Wenger, "Coupling emitters and silver nanowires to achieve long-range plasmon-mediated fluorescence energy transfer," *ACS Nano* **10**, 3968–3976 (2016).
38. C. Deeb, X. Zhou, R. Miller, S. K. Gray, S. Marguet, J. Plain, G. P. Wiederrecht, and R. Bachelot, "Mapping the electromagnetic near-field enhancements of gold nanocubes," *J. Phys. Chem. C* **116**, 24734–24740 (2012).
39. K. J. Schafer, J. M. Hales, M. Balu, K. D. Belfield, E. W. Van Stryland, and D. J. Hagan, "Two-photon absorption cross-sections of common photoinitiators," *J. Photochem. Photobiol. A* **162**, 497–502 (2004).
40. C. Deeb, R. Bachelot, J. Plain, A.-L. Baudrion, S. Jradi, A. Bouhelier, O. Soppera, P. K. Jain, L. Huang, C. Ecoffet, L. Balan, and P. Royer, "Quantitative analysis of localized surface plasmons based on molecular probing," *ACS Nano* **4**, 4579–4586 (2010).
41. C. Deeb, X. Zhou, J. Plain, G. P. Wiederrecht, R. Bachelot, M. Russell, and P. K. Jain, "Size dependence of the plasmonic near-field measured via single-nanoparticle photoimaging," *J. Phys. Chem. C* **117**, 10669–10676 (2013).
42. E. Fišerová and M. Kubala, "Mean fluorescence lifetime and its error," *J. Luminesc.* **132**, 2059–2064 (2012).
43. B. Gökbulut and M. N. Inci, "Enhancement of the spontaneous emission rate of Rhodamine 6G molecules coupled into transverse Anderson localized modes in a wedge-type optical waveguide," *Opt. Express* **27**, 15996–16011 (2019).
44. K. E. Knowles, E. A. McArthur, and E. A. Weiss, "A multi-timescale map of radiative and nonradiative decay pathways for excitons in CdSe quantum dots," *ACS Nano* **5**, 2026–2035 (2011).
45. F. M. Gómez-Campos and M. Califano, "Hole surface trapping in CdSe nanocrystals: dynamics, rate fluctuations, and implications for blinking," *Nano Lett.* **12**, 4508–4517 (2012).
46. O. Labeau, P. Tamarat, and B. Lounis, "Temperature dependence of the luminescence lifetime of single CdSe/ZnS quantum dots," *Phys. Rev. Lett.* **90**, 257404 (2003).
47. P. Spinicelli, S. Buil, X. Quélin, B. Mahler, B. Dubertret, and J.-P. Hermier, "Bright and grey states in CdSe-CdS nanocrystals exhibiting strongly reduced blinking," *Phys. Rev. Lett.* **102**, 136801 (2009).
48. Y. Peng, S. Jradi, X. Yang, M. Dupont, F. Hamie, X. Q. Dinh, X. W. Sun, T. Xu, and R. Bachelot, "3D photoluminescent nanostructures containing quantum dots fabricated by two-photon polymerization: influence of quantum dots on the spatial resolution of laser writing," *Adv. Mater. Technol.* **4**, 1800522 (2019).
49. A. Khalid, K. Chung, R. Rajasekharan, D. W. M. Lau, T. J. Karle, B. C. Gibson, and S. Tomljenovic-Hanic, "Lifetime reduction and enhanced emission of single photon color centers in nanodiamond via surrounding refractive index modification," *Sci. Rep.* **5**, 11179 (2015).
50. Q. Zhang, G. Li, X. Liu, F. Qian, Y. Li, T. C. Sum, C. M. Lieber, and Q. Xiong, "A room temperature low-threshold ultraviolet plasmonic nanolaser," *Nat. Commun.* **5**, 4953 (2014).